# Turbulence Models for Near-Wall and Low Reynolds Number Flows: A Review

Virendra C. Patel, Wolfgang Rodi, and Georg Scheuerer
*University of Karlsruhe, Karlsruhe, Federal Republic of Germany*

## I. Introduction

THE success enjoyed by the recent turbulence closure models in the prediction of wall-bounded shear flows has depended, to a large extent, upon the application of the so-called wall functions that relate surface boundary conditions to points in the fluid away from the boundaries and thereby avoid the problem of modeling the direct influence of viscosity. The validity of this procedure is, of course, restricted to situations in which the Reynolds number is sufficiently high for the viscous effects to be unimportant or where universal wall functions are well established. There are a number of instances in which this approach has to be abandoned, e.g., turbulent boundary layers at low and transitional Reynolds numbers, unsteady and separated flows, and the flow over spinning surfaces or surfaces with mass or heat transfer. Also, traditional wall functions are probably inappropriate for complex three-dimensional flows.

Over the past few years, many suggestions have been made for the extension of turbulence closure models to enable their use at low Reynolds numbers and to describe the flow close to a solid wall. The simplest example of a near-wall modification to a turbulence model is the van Driest[1] damping function for the mixing length. More advanced models incorporate either a wall damping effect or a direct effect of molecular viscosity, or both, on the empirical constants and functions in the turbulence-transport equations devised originally for high Reynolds number, fully turbulent flows remote from the walls. In the absence of reliable turbulence data in the immediate vicinity of a wall or at low Reynolds numbers, these modifications have been based largely upon numerical experiments and comparisons between calculations and experiments in terms of global parameters. Unfortunately, the results of each of the models were compared for different flows and it is not clear which of the many proposed models can be used with confidence.

This paper is concerned with a systematic evaluation of existing two-equation, "low Reynolds number" turbulence models. The limited but direct experimental evidence on the turbulence in the wall region is first reviewed. Eight different models are then summarized and the various assumptions and functions introduced to account for the low Reynolds number and wall-proximity effects are discussed. These models are then used, together with a single well-tested solution procedure, to calculate a variety of boundary layers. The test cases include not only boundary layers at low Reynolds numbers, but also the high Reynolds number and equilibrium boundary layers in adverse pressure gradients. The latter have been included specifically to ascertain that the extended models continue to perform at least as well as the parent models that were devised for such flows.

## II. Experimental Evidence

Experimental information pertaining to near-wall and low Reynolds number turbulence is rather limited and the data suffer from uncertainties arising from probe interference effects and the determination of the wall shear stress that provides the characteristic velocity and length scales. However, since all low Reynolds number models attempt to reproduce

**V. C. Patel received a B.Sc (Hons) degree in Aeronautics from Imperial College, London, in 1962 and a Ph.D. degree from Cambridge University, Cambridge, in 1965. After postdoctoral research at Cambridge, he was a consultant to the Lockheed-Georgia Research Laboratories, Marietta, Ga., during 1969-70. Since 1971 he has occupied various positions at The University of Iowa. Currently, he is Professor of Mechanical Engineering and Research Engineer at the Iowa Institute of Hydraulic Research. He is the author or coauthor of over 100 publications in turbulent boundary layers and shear flows, wind engineering, powerplant cooling systems and economics, and viscous ship hydrodynamics. Present research includes experimental and numerical investigations of complex three-dimensional turbulent flows with applications in aerodynamics and ship hydrodynamics. Dr. Patel is a Member of AIAA.**

**W. Rodi received a Diploma in Aeronautics from the University of Stuttgart, FRG, in 1966 and a Ph.D. degree in Mechanical Engineering from Imperial College, London, in 1973. During 1966-67 he was a NATO fellow at the University of Minnesota. In 1973 he joined the University of Karlsruhe, FRG, as Project Leader, and he is currently Professor of Civil Engineering at that university. His research has concentrated on the development of engineering calculation methods for turbulent flows and their application to a wide range of problems including flow and pollutant spreading in water bodies, aerodynamics, problems related to cooling towers, nuclear reactors, and turbine blade cooling. He is the author or coauthor of over 80 publications, including several monographs on turbulence modeling. He is a Member of AIAA.**

**G. Scheuerer received a Dipl.-Ing. degree from the Technical University of Munich in 1979 and a Dr.-Ing. degree from the University of Karlsruhe in 1983. He is presently a Research Engineer at the University of Erlangen-Nurnberg. His current research interests include the development and application of turbulence models for complex turbulent flows and the prediction of two-phase flows.**

Received July 13, 1984; revision received Oct. 1, 1984. 

some of the observed features of near-wall turbulence, it is useful to review the data, to the extent these are available. It should be noted that most of the available data have been obtained in flat-plate boundary layers or fully developed pipe flows and therefore we can supplement the data by some of the well-established correlations in these flows to guide the discussion.

### Turbulent Kinetic Energy

Coles[2] has compiled the existing near-wall data for the normal stresses $\overline{u^2}$, $\overline{v^2}$, and $\overline{w^2}$ that make up the turbulent kinetic energy $k$,

$$k = \tfrac{1}{2}(\overline{u^2} + \overline{v^2} + \overline{w^2}) \tag{1}$$

To these may be added the more recent measurements of El Telbany and Reynolds.[3] Figure 1a shows the resulting variation of $k^+$ $(= k/u_\tau^2)$ with $y^+$ $(= u_\tau y/\nu)$, where $u_\tau = \sqrt{\tau_w/\rho}$ is the friction velocity, $y$ the normal distance from the wall, and $\rho$ and $\nu$ the density and viscosity of the fluid, respectively. In spite of the rather large scatter, it is seen that $k^+$ becomes maximum around $y^+ = 15$, which corresponds to the location of the maximum production of $k$ (see Ref. 9). A representative peak value for $k^+$ is 4.5. In the interval $60 < y^+ < 150$, $k^+$ becomes almost constant and takes a value around 3.3. Since, in the log law region of a flat-plate boundary layer, the shear stress $-\overline{uv} \propto u_\tau^2$, the data suggest a value of around 0.3 for the structural coefficient $-\overline{uv}/k$, as found also in other shear layers.[4]

The variation of $k$ in the immediate vicinity of the wall can be deduced from the continuity equation and the no-slip condition. Following Launder,[5] the variation of the instantaneous velocity components with distance from the wall take the form

$$u = a_1 y + b_1 y^2 + \ldots \tag{2a}$$

$$v = \quad b_2 y^2 + \ldots \tag{2b}$$

$$w = a_3 y + b_3 y^2 + \ldots \tag{2c}$$

where the coefficients $a_i$ and $b_i$ are functions of time, but their time average is zero. Equations (2) lead to

$$k^+ = A^+ y^{+2} + B^+ y^{+3} + \ldots \tag{3a}$$

where

$$A^+ = \frac{\tfrac{1}{2}\nu^2}{u_\tau^4}(\overline{a_1^2} + \overline{a_3^2}) \tag{3b}$$

$$B^+ = \frac{\nu^3}{u_\tau^5}(\overline{a_1 b_1} + \overline{a_3 b_3}) \tag{3c}$$

The data of Kreplin and Eckelmann[6] support Eqs. (2) and suggest a value of 0.035 for $A^+$. Sirkar and Hanratty[7] give 0.05 at a higher Reynolds number, while the data compilation of Derksen and Azad[8] suggests $0.025 < A^+ < 0.05$, with the higher values occurring at larger Reynolds numbers.

The first term in Eq. (3a) with $A^+ = 0.05$ is shown in Fig. 1a. The mean line through the data shown in the figure is used later for direct comparison with the calculations.

### Shear Stress

Figure 1b shows the distribution of the shear stress $-\overline{uv}^+$ $(= -\overline{uv}/u_\tau^2)$ in the near-wall region according to the data collected by Coles.[2] In addition, the data of Schubauer[10] are plotted. Note that the Reynolds stress accounts for approximately 50% of the total stress at $y^+ \approx 10$. In the log law region of turbulent flows with small pressure gradients, the

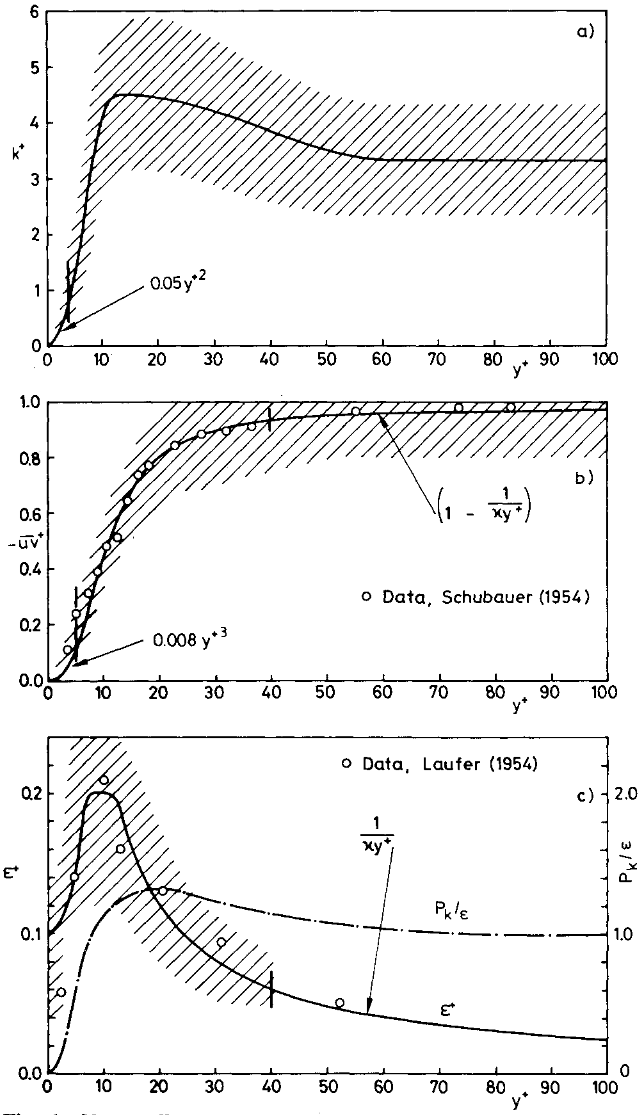


**Fig. 1 Near-wall variation of the turbulence quantities: a) turbulent kinetic energy $k$; b) Reynolds stress $-\overline{uv}$; c) dissipation rate $\epsilon$.**

momentum equation yields

$$-\overline{uv}^+ = 1 - (1/\kappa y^+) \tag{4}$$

where $\kappa$ is the von Kármán constant. Very close to the wall, however, Eqs. (2) suggest

$$-\overline{uv}^+ \propto y^{+3} \tag{5}$$

The solid line in Fig. 1b has been drawn with these asymptotes and is seen to be in good agreement with the data.

### Dissipation Rate

The dissipation rate used in the $k$-$\epsilon$ model is defined as

$$\epsilon = \nu \overline{\frac{\partial u_j}{\partial x_i}\frac{\partial u_j}{\partial x_i}} \tag{6}$$

which, as Hinze[4] points out, is the dissipation rate only in the case of homogeneous turbulence. However, most authors do not make this distinction. For the present purposes, Eq. (6) is adopted since it is consistent with the models of the turbulent kinetic energy equation introduced later.

The available data for the distribution of the dissipation rate in the near-wall region are quite limited and are all subject to a large measurement uncertainty, especially in the region $0<y^+<40$. Figure 1c shows the data collected by Coles along with those of Laufer.[11]

The distribution of $\epsilon$ can also be inferred from considerations similar to those for $k$ and $-\overline{uv}$. In the log law region $40<y^+<100$, say, production of $k$ is roughly equal to the dissipation. Since production is

$$P_k = -\overline{uv}\frac{\partial U}{\partial y} \tag{7}$$

the velocity gradient from the logarithmic law,

$$U^+ = (1/\kappa)\ln y^+ + C \tag{8}$$

and $-\overline{uv}\approx u_\tau^2$ lead to

$$\epsilon^+ = \frac{\nu\epsilon}{u_\tau^4} = \frac{1}{\kappa y^+} \tag{9}$$

Very close to the wall, substitution of Eqs. (2) into Eq. (6) yields[5]

$$\epsilon^+ = 2(A^+ + 2B^+ y^+ + \ldots) \tag{10}$$

indicating a finite $\epsilon$ at the wall equal to $2A^+$. Experimental values of $A^+$ quoted earlier then indicate $0.05<\epsilon_w<0.10$, with a preference for the higher value at larger Reynolds numbers. If $B^+=0$ is assumed, Eq. (10) indicates

$$y^+ = 0: \frac{\partial \epsilon^+}{\partial y^+} = 0 \tag{11}$$

which can be used as a boundary condition for $\epsilon$.

The solid line in Fig. 1c has been drawn as a mean curve through the data, taking into consideration the limiting behavior noted above.

#### Velocity Gradient

The velocity gradient in the wall region may be calculated with the aid of van Driest's[1] mixing length formula, which, together with the assumption of constant total stress, yields

$$\frac{dU^+}{dy^+} = \frac{-1+\sqrt{1+4(\kappa y^+ D^*)^2}}{2(\kappa y^+ D^*)^2} \tag{12}$$

where $D^*=1-\exp(-y^+/A^*)$ and $A^*=25.6$ gives $C=5.2$ in the log law.[8] Using the velocity gradient from Eq. (12), the Reynolds stress from Fig. 1b and therefore $P_k$ from Eq. (7), and the data of Laufer for $\epsilon$, the ratio $P_k/\epsilon$ can be determined. This is also shown in Fig. 1c. Note that the assumption of local equilibrium in the log law region, i.e., $P_k/\epsilon=1$, is then recovered.

## III. Outline of Near-Wall Models

Eight models, namely those of Chien,[12] Dutoya and Michard,[13] Hassid and Poreh,[14] Hoffmann,[15] Lam and Bremhorst,[16] Launder and Sharma,[17] Reynolds,[18] and Wilcox and Rubesin[19] were selected for a detailed evaluation. The first seven are variants of the $k$-$\epsilon$ model, in which the Reynolds stress is related to the local velocity gradient by an eddy viscosity $\nu_t$, which is computed from modeled transport equations for $k$ and $\epsilon$. Wilcox and Rubesin[19] employ an equation for the kinetic energy of the normal velocity fluctuations, together with a transport equation for a pseudovorticity $\omega$. The relevant equations of the models for two-dimensional boundary layers are:

$$-\rho\overline{uv} = \rho\nu_t\frac{\partial U}{\partial y} \tag{13}$$

$k$-$\epsilon$ model:

$$\nu_t = c_\mu f_\mu \frac{k^2}{\tilde{\epsilon}} \tag{14}$$

$$\epsilon = \tilde{\epsilon} + D \tag{15}$$

$$U\frac{\partial k}{\partial x} + V\frac{\partial k}{\partial y} = \frac{\partial}{\partial y}\left[\left(\nu+\frac{\nu_t}{\sigma_k}\right)\frac{\partial k}{\partial y}\right] + \nu_t\left(\frac{\partial U}{\partial y}\right)^2 - \epsilon \tag{16}$$

$$U\frac{\partial \tilde{\epsilon}}{\partial x} + V\frac{\partial \tilde{\epsilon}}{\partial y} = \frac{\partial}{\partial y}\left[\left(\nu+\frac{\nu_t}{\sigma_\epsilon}\right)\frac{\partial \tilde{\epsilon}}{\partial y}\right] + c_{\epsilon 1}f_1\frac{\tilde{\epsilon}}{k}\nu_t\left(\frac{\partial U}{\partial y}\right)^2 - c_{\epsilon 2}f_2\frac{\tilde{\epsilon}^2}{k} + E \tag{17}$$

$$R_T = k^2/\nu\tilde{\epsilon} \tag{18}$$

$$R_y = \sqrt{k}y/\nu \tag{19}$$

$$y^+ = yu_\tau/\nu \tag{20}$$

$k$-$\omega$ model:

$$\nu_t = f_\mu(k/\omega) \tag{21}$$

$$U\frac{\partial k}{\partial x} + V\frac{\partial k}{\partial y} = \frac{\partial}{\partial y}\left[\left(\nu+\frac{\nu_t}{\sigma_k}\right)\frac{\partial k}{\partial y}\right] + \nu_t\left(\frac{\partial U}{\partial y}\right)^2 - c_\mu k\omega \tag{22}$$

$$U\frac{\partial \omega^2}{\partial x} + V\frac{\partial \omega^2}{\partial y} = \frac{\partial}{\partial y}\left[\left(\nu+\frac{\nu_t}{\sigma_\omega}\right)\frac{\partial \omega^2}{\partial y}\right] + c_{\omega 1}f_1\omega\left(\frac{\partial U}{\partial y}\right)^2 - c_{\omega 2}\omega^3 + E \tag{23}$$

$$l = \sqrt{k}/\omega \tag{24}$$

$$R_T = \sqrt{k}l/\nu \tag{25}$$

Table 1 summarizes the low Reynolds number functions for the $k$-$\epsilon$ group of models. The first line in the table is the parent high Reynolds number model (HR) and contains also the five basic constants. Table 2 summarizes the model of Wilcox and Rubesin. In these equations, $x$ is in the streamwise direction, $y$ is normal to the wall, and $U, V$ are the corresponding mean velocity components. In the interest of brevity, the various models will henceforth be referred to by the letter codes indicated in Tables 1 and 2 (e.g., Chien is CH, etc.).

The models in the $k$-$\epsilon$ group differ from their basic version by the inclusion of the viscous diffusion terms and of functions $f$ to modify the constants $c$. Also, extra terms, denoted by $D$ and $E$, are added in some cases to better represent the near-wall behavior. The similarity between these models and that of Wilcox and Rubesin (WR) is apparent from Tables 1 and 2. The different proposals are examined below in light of the physical and experimental evidence summarized in the previous section.

**Table 1 Constants and functions for the $k$-$\epsilon$ group of models**

| Model | Code | $D$ | $\tilde{\epsilon}_w$-B.C. | $c_\mu$ | $c_{\epsilon 1}$ | $c_{\epsilon 2}$ | $\sigma_k$ | $\sigma_\epsilon$ |
|---|---|---|---|---|---|---|---|---|
| Standard | HR | 0 | Wall functions | 0.09 | 1.44 | 1.92 | 1.0 | 1.3 |
| Launder-Sharma | LS | $2\nu\left(\frac{\partial\sqrt{k}}{\partial y}\right)^2$ | 0 | 0.09 | 1.44 | 1.92 | 1.0 | 1.3 |
| Hassid-Poreh | HP | $2\nu\frac{k}{y^2}$ | 0 | 0.09 | 1.45 | 2.0 | 1.0 | 1.3 |
| Hoffman | HO | $\frac{\nu}{y}\frac{\partial k}{\partial y}$ | 0 | 0.09 | 1.81 | 2.0 | 2.0 | 3.0 |
| Dutoya-Michard | DM | $2\nu\left(\frac{\partial\sqrt{k}}{\partial y}\right)^2$ | 0 | 0.09 | 1.35 | 2.0 | 0.9 | 0.95 |
| Chien | CH | $2\nu\frac{k}{y^2}$ | 0 | 0.09 | 1.35 | 1.8 | 1.0 | 1.3 |
| Reynolds | RE | 0 | $\nu\frac{\partial^2 k}{\partial y^2}$ | 0.084 | 1.0 | 1.83 | 1.69 | 1.3 |
| Lam-Bremhorst | LB | 0 | $\nu\frac{\partial^2 k}{\partial y^2}$ | 0.09 | 1.44 | 1.92 | 1.0 | 1.3 |
| Lam-Bremhorst | LB1 | 0 | $\frac{\partial\epsilon}{\partial y}=0$ | 0.09 | 1.44 | 1.92 | 1.0 | 1.3 |

| Code | $f_\mu$ | $f_1$ | $f_2$ | $E$ |
|---|---|---|---|---|
| HR | 1.0 | 1.0 | 1.0 | 0 |
| LS | $\exp\left[\frac{-3.4}{(1+R_T/50)^2}\right]$ | 1.0 | $1-0.3\exp(-R_T^2)$ | $2\nu\nu_t\left(\frac{\partial^2 U}{\partial y^2}\right)^2$ |
| HP | $1-\exp(-0.0015R_T)$ | 1.0 | $1-0.3\exp(-R_T^2)$ | $-2\nu\left(\frac{\partial\sqrt{\tilde{\epsilon}}}{\partial y}\right)^2$ |
| HO | $\exp\left(\frac{-1.75}{1+R_T/50}\right)$ | 1.0 | $1-0.3\exp(-R_T^2)$ | 0 |
| DM | $1-0.86\exp\left[-\left(\frac{R_T}{600}\right)^2\right]$ | $1-0.04\exp\left[-\left(\frac{R_T}{50}\right)^2\right]+0.25\left(\frac{\lambda}{y}\right)^2$ | $1-0.3\exp\left[-\left(\frac{R_T}{50}\right)^2\right]-0.08\left(\frac{\lambda}{y}\right)^2$ | $-c_{\epsilon 2}f_2(\tilde{\epsilon}D/k)$ [a] |
| CH | $1-\exp(-0.0115y^+)$ | 1.0 | $1-0.22\exp[-(R_T/6)^2]$ | $-2\nu(\tilde{\epsilon}/y^2)\exp(-0.5y^+)$ |
| RE | $1-\exp(-0.0198R_y)$ | 1.0 | $\{1-0.3\exp[-(R_T/3)^2]\}h(R_y)$ | 0 |
| LB | $[1-\exp(-0.0165R_y)]^2\times\left(1+\frac{20.5}{R_T}\right)$ | $1+(0.05/f_\mu)^3$ | $1-\exp(-R_T^2)$ | 0 |
| LB1 | $[1-\exp(-0.0165R_y)]^2\times\left(1+\frac{20.5}{R_T}\right)$ | $1+(0.05/f_\mu)^3$ | $1-\exp(-R_T^2)$ | 0 |

[a] $\tilde{\epsilon}\to\epsilon$ in Eqs. (19) and (23).

**Table 2 Constants and functions for the model of Wilcox and Rubesin (WR)[19]**

| | | | |
|---|---|---|---|
| $c_\mu$ | 0.09 | $\sigma_\omega$ | 2.0 |
| $c_{\omega 1}$ | 1.11 | $f_\mu$ | $1-0.992\exp(-R_T)$ |
| $c_{\omega 2}$ | 0.15 | $f_1$ | $1-0.992\exp(-R_T/2)$ |
| $\sigma_k$ | 2.0 | $E$ | $-\frac{2}{\sigma_\omega}\left(\frac{\partial l}{\partial y}\right)^2\omega^3$ |

**Table 3 Near-wall values of the term $D$**

| $D$ | Resulting near-wall value of $\epsilon^+$ |
|---|---|
| $2\nu(k/y^2)$ | $(2A^+ + 2B^+y^+)$ |
| $\frac{\nu}{y}\frac{\partial k}{\partial y}$ | $(2A^+ + 3B^+y^+)$ |
| $2\nu\left(\frac{\partial\sqrt{k}}{\partial y}\right)^2$ | $(2A^+ + 4B^+y^+)$ |

**The $k$-$\epsilon$ Group of Models**

Consider the seven modifications to the $k$-$\epsilon$ model listed in Table 1. We note that only RE and LB employ a transport equation for the dissipation rate $\epsilon$ itself, while the remaining models solve for a quantity $\tilde{\epsilon}=\epsilon-D$. The implications of this will be discussed first.

*The Dissipation Variable*

The proposal of using $\tilde{\epsilon}$ as the "dissipation variable" is due to Jones and Launder,[20] who cited decisive computational advantages because $D$ is chosen such that $\tilde{\epsilon}=0$ at the wall, a numerically convenient boundary condition. Not all authors employ the same term $D$, however; three different proposals appear in Table 1. If $\tilde{\epsilon}=0$ is specified as a wall boundary condition (see column 4 of Table 1), the term $D$ must asymptote to the nonzero value of $\epsilon$ at the wall, discussed earlier, in order to keep the $k$ equation in balance. This can be verified by substituting Eq. (3) into the different proposals for $D$. Table 3 shows the corresponding results. It is seen that all proposals yield the correct wall value of $\epsilon$, namely $2A^+$ in Eq. (10), but only the formulas by LS and DM give the proper coefficient for the linear term as well. However, in the immediate vicinity of the wall, the Reynolds stress (for the determination of which $\tilde{\epsilon}$ is needed) is small in comparsion with the viscous stress and therefore the differences are of little consequence. More important is the criterion that in the fully turbulent regime, say, $y^+>60$, $\tilde{\epsilon}$ should be equal to the dissipation rate $\epsilon$ used in the basic $k$-$\epsilon$ model. This means that $D$ must vanish in this zone. If values of $k$, $\partial k/\partial y$, and $\epsilon$ at $y^+=60$ are taken from the curves in Fig. 1, it is found that $D/\epsilon$ is 0.055 for the models of HP and CH, while it is almost negligible in the other cases. Also, the $D$ term of HO becomes negative beyond the peak in $k$, so that $\tilde{\epsilon}$ is different from $\epsilon$, although by numerically small amounts.

As noted above, Jones and Launder selected $\tilde{\epsilon}$ as the dissipation variable for numerical convenience. However, $\tilde{\epsilon}$ varies very rapidly near the wall. If, for example, the distributions of $k$ and $\tilde{\epsilon}$ in the region $0<y^+<10$ in Fig. 1 are approximated by straight lines, we have $\partial\epsilon/\partial y=0.02u_\tau^2/\nu^2$ and $\partial k/\partial y=0.4u_\tau^3/\nu$ so that the ratio $(\partial\epsilon/\partial y)/(\partial k/\partial y)=0.05u_\tau^2/\nu$ is of the order of $10^3$ for air. Thus, compared to the kinetic energy $k$ (or the velocity $U$), $\tilde{\epsilon}$ increases at a much faster rate with wall distance. It is difficult to numerically resolve this rapid growth with sufficient accuracy and the solutions may not be grid independent near the wall. These problems are alleviated to some extent by using a transport equation for the dissipation rate $\epsilon$ since the gradients of $\epsilon$ are much smaller. Also, for a physical point of view, it is more attractive to use an equation for the dissipation rate itself. This approach has been followed by LB and RE.

The associated problem of specifying a wall boundary condition for $\epsilon$ has been resolved by LB and RE by using the $k$ equation at the wall, i.e., $\epsilon_w=\nu\partial^2k/\partial y^2$. Although this has been used in numerical solution procedures, it is not very convenient since it involves parts of the solution of the system of coupled differential equations. A more convenient boundary condition for $\epsilon$ is that its gradient vanishes at the wall as indicated by Eq. (11). The wall value $\epsilon_w$ is then a result of the calculation. Hanjalic and Launder[21] have used this boundary condition in calculations with a Reynolds-stress-equation model. It has been used in this study in connection with the model of LB (denoted by LB1 in Table 1).

*Model Constants*

Columns 5-9 in Table 1 contain the five empirical constants $c_\mu$, $c_{\epsilon 1}$, $c_{\epsilon 2}$, $\sigma_k$, and $\sigma_\epsilon$ used in the different models. For high-turbulence Reynolds numbers $R_T$ or $R_y$, the functions $f_\mu$, $f_1$, and $f_2$ multiplying the first three constants tend to unity; therefore, the model behavior depends only on the values of the five constants. The first line in Table 1 shows the constants for the standard model.[22] They have been tested in a variety of free shear layers and, together with wall functions, for boundary layers and confined flows.

Table 1 shows little diversity in the constants $c_\mu$ and $c_{\epsilon 2}$ determined from experimental data in near-wall and isotropic turbulence, respectively. Larger differences are apparent in the values of $c_{\epsilon 1}$, $\sigma_k$, and $\sigma_\epsilon$, which are usually obtained by computer optimization. Not all sets of constants satisfy the relation

$$c_{\epsilon 1}=c_{\epsilon 2}-(\kappa^2/\sigma_\epsilon c_\mu^{1/2}) \tag{26}$$

to which the $\epsilon$ equation reduces in zero pressure gradient local-equilibrium flows with a logarithmic velocity distribution. The constants of HP and RE imply values of 0.463 and 0.570 for the von Kármán constant $\kappa$, well above the accepted value of $0.41\pm0.015$. The differences in the constants may be quite significant insofar as they contribute to the overall performance of the models.

Extensive calculations of free shear layers by Launder et al.[23] indicate that, at least for these flows, the results are indeed very sensitive to the precise values of $c_{\epsilon 1}$ and $c_{\epsilon 2}$. This was confirmed in the present work, where the high Reynolds number asymptotes ($f_\mu=f_1=f_2=1$; $D=E=0$) were utilized to calculate the asymptotic spreading rate of a plane mixing layer. Table 4 compares the results with the mean experimental value suggested by Rodi.[24] It is clear that the models of HO, DM, and RE do not possess the degree of generality usually associated with a two-equation turbulence model and can, at best, be regarded as specifically tailored near-wall models.

*The Function $f_\mu$*

Function $f_\mu$ multiplies the eddy viscosity relation[14] and is introduced to mimic the direct effect of molecular viscosity on the shear stress. Launder[25] notes that the shear stress near the wall is also reduced by the action of the fluctuating pressure field via the pressure strain correlation. This process

**Table 4 Asymptotic spreading rates of turbulent mixing layers**

| $d\delta/dx$ | Model | $d\delta/dx$ | Model | $d\delta/dx$ | Model |
|---|---|---|---|---|---|
| 0.16 | Exp. | 0.17 | HP | 0.15 | CH |
| 0.15 | HR | 0.05 | HO | 0.28 | RE |
| 0.15 | LS | 0.20 | DM | 0.15 | LB |

**Table 5 Limiting values for the function $f_\mu$**

| Model | $y^+(f_\mu=0.95)$ | Model | $y^+(f_\mu=0.95)$ |
|---|---|---|---|
| LS | 78.4 | CH | 260.5 |
| HP | 438. | RE | 82.9 |
| HO | 363.5 | LB | 102.4 |
| DM | 222.1 | | |

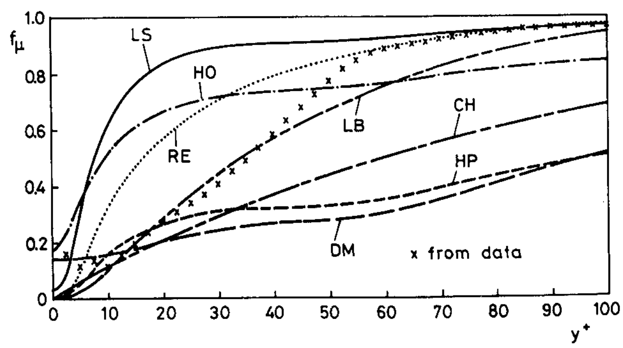


**Fig. 2 Variation of the function $f_\mu$ with wall distance.**

is, to a first approximation, independent of viscosity and, therefore, cannot be correlated by the Reynolds numbers $R_T$, $R_y$, or $y^+$. However, it is difficult to separate the two effects as both occur in the vicinity of a wall. The $f_\mu$ functions thus attempt to model both the viscous and pressure strain effects, although they are properly correlated only for the former.

The various proposals for $f_\mu$ can be examined according to three criteria: 1) comparison with a distribution constructed from the experimental data; 2) their influence in the logarithmic region, and 3) the implied near-wall distributions of $-\overline{uv}$. The last is perhaps the least critical, as the turbulent stress is small compared to the viscous stress in the immediate vicinity of the wall.

From Eqs. (13) and (14), we obtain

$$f_\mu = \frac{-\overline{uv}^+ \epsilon^+}{c_\mu k^{+2}(\mathrm{d}U^+/\mathrm{d}y^+)} \tag{27}$$

The "experimental" curve for $f_\mu$, which results when the data of Fig. 1 are substituted in this equation, is shown in Fig. 2. It exhibits an almost constant value for $y^+ < 15$, an approximately linear increase up to $y^+ = 60$ and a gradual approach toward unity. If the Reynolds numbers $R_T = (k^+)^2/\epsilon^+$ and $R_y = \sqrt{k^+}y^+$ are calculated from the data of Fig. 1, the various proposals for $f_\mu$ can be compared with the "experimental" curve, as is shown in Fig. 2. It is clear that none of the model functions follows the distribution suggested by the data over the whole range of $y^+$. The function selected by LB is a good approximation in the viscous zone ($y^+ < 40$); the formulas of LS and RE yield relatively high values there, but show better agreement with the "experimental" curve in the fully turbulent regime ($y^+ > 40$). The functions of HP, DM, and CH increase too slowly with wall distance to match the empirical distribution. The differences in Fig. 2 may be explained by the fact that $f_\mu$ has been determined by computer optimization in all cases rather than by recourse to experimental data.

The second criterion for $f_\mu$ relates to the behavior in the fully turbulent logarithmic layer where $f_\mu$ must tend to unity if the parent high Reynolds number model is to be recovered. Experimental data suggest that the viscous effects become negligible for $y^+ > 60$, whereas Fig. 2 shows that the various functions reach an asymptotic value of 1 well beyond $y^+ = 60$. In the fully turbulent zone, the data indicate that $R_T$ and $R_y$ follow approximately

$$R_T = 4.56y^+; \quad R_y = 1.83y^+ \tag{28}$$

If these relations are inserted into the proposed $f_\mu$ formulas, the values of $y^+$ at which $f_\mu = 0.95$ are as shown in Table 5. It is apparent that in the models of HP, HO, DM, and CH a wall damping effect prevails out to unrealistically large wall distances. It should be noted that the wall functions used in connection with the standard model (with $f_\mu = 1$) are usually applied in a region $30 < y^+ < 200$.

**Table 6 Exponents of the near-wall variation of the turbulence quantities**

| Model | LS | HP | HO | DM | CH | RE | LB |
|---|---|---|---|---|---|---|---|
| $\tilde{\epsilon}$ | 1 | 2 | 1 | 2 | 2 | 0 | 0 |
| $k^2/\tilde{\epsilon}$ | 3 | 2 | 3 | 2 | 2 | 4 | 4 |
| $f_\mu$ | 0 | 2 | 0 | 0 | 1 | 2 | 0 |
| $L = k^{3/2}/\tilde{\epsilon}$ | 2 | 1 | 2 | 1 | 1 | 3 | 3 |
| $-\overline{uv}$ | 3 | 4 | 3 | 4 | 3 | 6 | 4 |

Prior to an assessment of the third criterion dealing with the near-wall distribution of the Reynolds stress, the $\epsilon$ equation at the wall has to be inspected. It reads

$$\nu\frac{\partial^2\tilde{\epsilon}}{\partial y^2} = c_{\epsilon 2}f_2\frac{\tilde{\epsilon}^2}{k} + E = 0 \tag{29}$$

If $\epsilon = ay + by^2 + cy^3$ is substituted in Eq. (29), the linear term has to be dropped in some models to satisfy it. This feature depends on the form of the extra term $E$. With $k \propto y^2$ and a series expansion of $f_\mu$, it is possible to calculate the exponent $n$ in $-\overline{uv} \propto y^n$. These exponents are compiled in Table 6. For models using an equation for $\epsilon$ itself, $\epsilon = \epsilon_w + by^2 + cy^3$ is valid and, in the absence of extra terms $E$, $f_2 \propto y^2$ is necessary to render the $\epsilon$ equation consistent at the wall. Not all models yield $n = 3$ as demanded by Eq. (5). (A value of $n = 4$ would be demanded if the correlation coefficient between $u$ and $v$ approaches zero at the wall; unfortunately, the available data on this correlation coefficient at the wall are insufficient to discern between $n = 3$ and 4.) HP, DM, and LB give $n = 4$, which agrees with the successful mixing length formula of van Driest,[1] while the value $n = 6$ in RE is unrealistically high.

*The Function $f_2$*

Function $f_2$ is introduced primarily to incorporate low Reynolds number effects in the destruction term of the $\epsilon$ equation. The physical basis for this is provided by experiments in the final period of the decay of isotropic turbulence, which show that the exponent in the decay law $k \propto x^{-n}$ changes from 1.25 at high Reynolds numbers to 2.5 in the final stage. The latter number is exactly met by the models of HP, HO, DM, and CH, whereas the versions of LS and RE imply a slower decay. The most elaborate fit to the data of Batchelor and Townsend[26] is achieved by CH's function, which originates from the work of Hanjalic and Launder.[21] The fact that all formulas reach their asymptotic value of unity at Reynolds numbers $R_T$ smaller than 15 leads to the conclusion that their effect is limited to the viscous sublayer and that nuances in the shapes of $f_2$ will not exert a large influence on the overall results. As mentioned above, consistency of the models of RE and LB with the $\epsilon$ equation require $f_2 \propto y^2$ in the vicinity of the wall. Although the zero value of $f_2$ at the wall is attained in the case of LB by simply omitting the factor 0.3 in the function of LS, none of these proposals satisfies $f_2 \propto y^2$. Moreover LB's model excludes the prediction of the final stage of isotropic turbulence. In this regard, RE's function is more general and preferable (unfortunately RE did not specify an empirical constant in the $f_2$ function and therefore the model could not be used in the subsequent calculations).

Table 1 shows that DM introduce a direct effect of the wall proximity on $f_2$ that reduces the destruction term and thereby increases the absolute value of $\epsilon$. They employ the Taylor microscale as a scaling parameter, which is approximated by $\lambda = \sqrt{10\nu k/\epsilon}$. The term $0.08\ (\lambda/y)^2$ appearing in the model is of the order of 0.4 in the viscous sublayer. Therefore, $f_2$ is positive, although the formula does not exclude negative values.

*The Function $f_1$ and the Extra Term $E$*

Several models employ an additional empirical term $E$ and/or function $f_1$ in the $\epsilon$ equation. In the models of HP, CH, and DM, $E$ is introduced to yield a quadratic growth of $\epsilon$ with wall distance. The expression for $E$ in the model of LS vanishes in the viscous sublayer and decreases with $y^4$ in the logarithmic region. Consequently, the maximum is located in the buffer layer. The term is then likely to increase the dissipation rate in this region, which results in a lower peak of $k$. A similar effect is achieved by the $f_1$ functions of DM and LB. Both increase the magnitude of $\epsilon$ near the wall.

### The Model of Wilcox and Rubesin (WR)

The basic equations of this model are Eqs. (21-25) and the modifications are cited in Table 2. WR employ an equation which is very similar to the $k$ equation (16) for determining the velocity scale in the eddy viscosity relation [Eq. (21)]. However, they interpret $k$ as a mixing energy more akin to the normal component of the Reynolds stress, viz $k \approx 9/2\ \overline{v^2}$. Since a direct relationship with the turbulent kinetic energy is now absent, it is difficult to make comparisons with conventional turbulence measurements. The same is true for the length scale determining variable $\omega$, which is proportional to the ratio of dissipation to turbulent kinetic energy, according to

$$\omega = \frac{1}{c_\mu}\frac{\epsilon}{k} \tag{30}$$

*The Length Scale Variable $\omega$*

Attention is first drawn to the near-wall behavior and the boundary conditions. In the $k$-$\epsilon$ model, the latter are fixed by the known behavior of the physical quantities. In the WR model, this is not feasible and greater freedom is exercised in setting these values. In fact, the boundary value of $\omega$ at the wall is made a function of parameters such as roughness and blowing rates. For smooth, impermeable walls, WR specify

$$\omega_w^+ = \frac{\omega\nu}{u_\tau^2} = \frac{20}{c_{\omega 2} y^{+2}} \tag{31}$$

which implies an infinite value at a rigid boundary. This leaves considerable freedom in numerical calculations since a "large" value can be assigned. However, it became apparent in the present work that the computed results depended on the actual value specified. Since WR do not recommend any particular value, the calculations presented later were made with $y^+ = 0.2$ in Eq. (31); smaller $y^+$ did not yield satisfactory results. This uncertainty in setting the boundary conditions must be considered a shortcoming of the model. Writing the $k$ equation (22) at the wall

$$\frac{\partial^2 k}{\partial y^2} = c_\mu k\omega \tag{32}$$

and introducing the limiting equation (31) for $\omega$, it follows that $k \propto y^4$ is implied near the wall. This behavior shows the close resemblance of $k$ with $\overline{v^2}$ [see Eq. (2b)]. From Eq. (30), it follows that $\epsilon$ is zero at the wall in this model, which is not in agreement with the behavior of the physical dissipation rate. Moreover, Eq. (24) yields a finite value of the length scale at the wall.

Inspection of the $\omega^2$ equation shows that, at the wall, the diffusion and destruction terms balance, but both go to infinity as $y^{-6}$. Thus, differences of very large numbers are involved in the $\omega^2$ equation presenting some numerical problems.

With regard to the freestream boundary conditions, some algebra shows that both turbulence model equations are satisfied in the limit of large $y$ by $k \propto x^{-m}$ with $m = -2c_\mu \div c_{\omega 2} = 1.2$. The boundary conditions specified by WR do not follow this relation and are therefore inconsistent with the differential equations.

*The Function $f_\mu$*

A direct comparison with experimental values is not meaningful in this case. However, it is interesting to examine the implications of $f_\mu$ in the logarithmic region and very close to the wall. If $R_T = y^+$, which is valid under local equilibrium conditions, is applied at $y^+ = 30$ (approximately the lower limit of its applicability), the value of $f_\mu$ is very close to unity. This means that the damping effect of $f_\mu$ is restricted to the viscous sublayer and the buffer region. Also, if the near-wall distributions of $k$ and $\omega$ discussed above are combined, the near-wall behavior of the various quantities is as shown in Table 7. It is seen that this model yields $-uv \propto y^6$, a fairly high exponent compared with the experimental value of 3 [Eq. (5)].

*The Function $f_l$ and the Extra Term $E$*

The function $f_l$ reduces the generation term in the $\omega^2$ equation at low-turbulence Reynolds numbers and is therefore likely to promote higher values of $\mu_t$ and $-\overline{uv}$. This feature is contrary to what may be expected under these conditions. Finally, the term $E$, named gradient dissipation, appears in the $\omega^2$ equation. It stems from a comparison with the $\epsilon$ equation (see Ref. 27) and ensures the correct behavior of the length scale in the outer part of boundary layers.

### Conclusions

The foregoing discussion shows that most modifications to the basic high Reynolds number turbulence models lack a sound physical basis. The choice of the dissipation variable $\tilde{\epsilon}$ does not seem to be crucial for the success or failure of a model as long as the wall boundary condition for $\tilde{\epsilon}$ is formulated in a consistent way, as is the case for all models. On the other hand, the choice of the empirical constants in the

**Table 7 Near-wall variation of the turbulence quantities in the model of Wilcox and Rubesin (WR)[19]**

| Quantity | $\omega$ | $k/\omega$ | $f_\mu$ | $l = \sqrt{k}/\omega$ | $-\overline{uv}$ |
|---|---|---|---|---|---|
| Exponent $n$ of $\Phi \propto y^n$ | $-2$ | 6 | 0 | 4 | 6 |

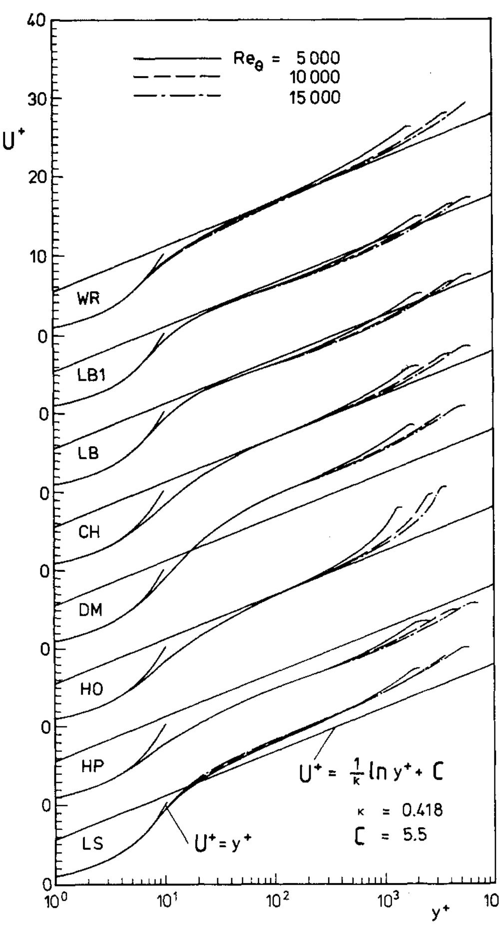


**Fig. 3 Calculated velocity profiles at different Reynolds numbers.**

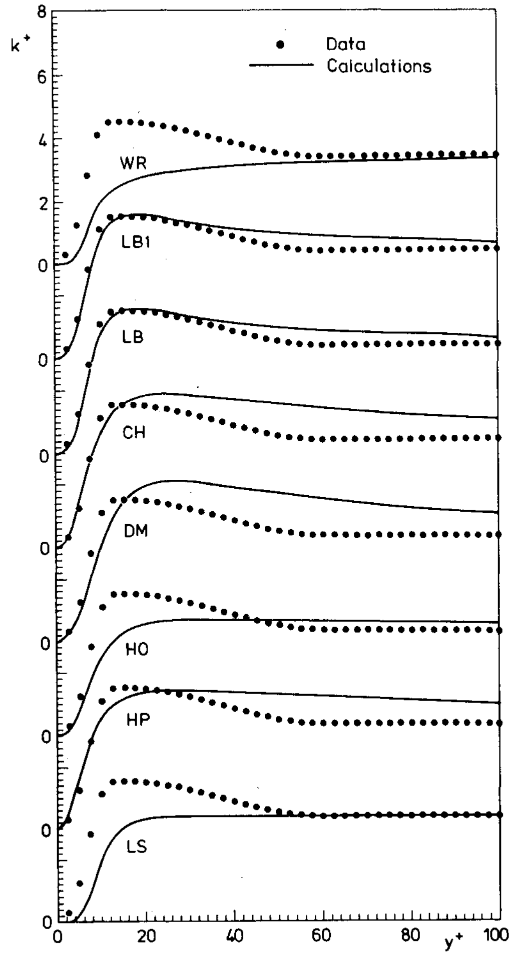


**Fig. 4 Measured and calculated turbulent kinetic energy profiles in the near-wall region.**

high Reynolds number parent model has much bearing on the general applicability of the low Reynolds number versions. It has been demonstrated that the constants in the models of HP, HO, DM, and RE restrict their generality.

It is difficult to provide a rating of the low Reynolds number functions purely on the basis of the experimental evidence. However, the $f_\mu$ function has a predominant influence on the model performance. The functions in the models of HP, HO, DM, and CH are unrealistic insofar as a wall damping influence exists even at very large wall distances. The differences in the functions $f_1$ and $f_2$, and in the extra terms $E$, appear to play a secondary role. It should be remarked that the $f_2$ function in the LB model does not allow one to simulate the decay of grid turbulence, but it could easily be modified to do so. Several inconsistencies in the near-wall behavior of the turbulence quantities have been pointed out for the WR model. However, as a direct relationship with the physical quantities is not claimed, the effects of these inconsistencies should not be exaggerated.

In the absence of reliable pertinent data, support for the models has been provided largely by comparison of calculations with the gross parameters of shear layers. However, only the models of LS (and the closely related model by Jones and Launder) and WR have been used extensively. The former has been used over a much wider range of flows, including free shear layers, while the latter has been employed for boundary layers with special emphasis on compressible flows.

## IV. Selection of Test Cases

Before describing the results of the calculations, it is necessary to discuss two aspects that may influence the conclusions. The first concerns the criteria by which success or failure is to be judged. Among those considered important are 1) the model should reproduce results of the parent high Reynolds number model for flows not dominated by low Reynolds numbers; and 2) the model predictions in the wall region, and for flows in which low Reynolds number effects

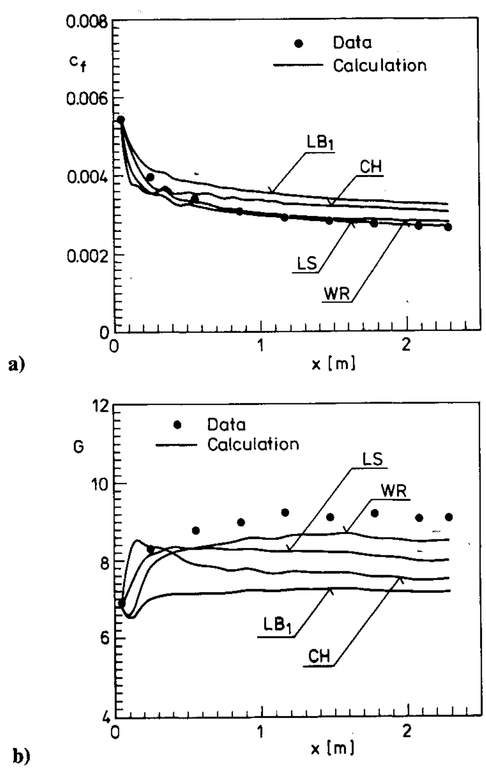


**Fig. 5 Comparison of model results with the data of Andersen et al.[29]: a) skin-friction coefficients; b) equilibrium shape parameters.**

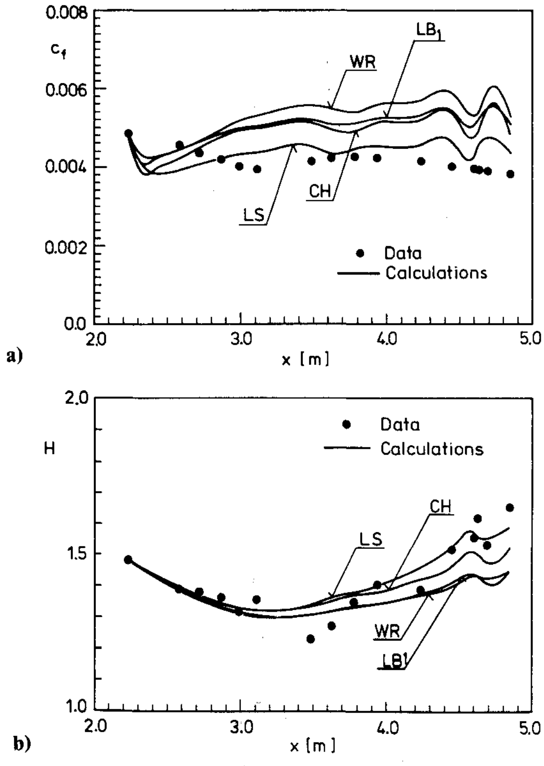


**Fig. 6 Comparison of model results with the data of Simpson and Wallace[30]: a) skin-friction coefficients; b) shape factors $H$.**

**Table 8 Skin-friction coefficients for the experiment of Wieghardt and Tillmann[28]**

| Quantity | Experiment | LS | HP | HO | DM | CH | LB | LB1 | WR |
|---|---|---|---|---|---|---|---|---|---|
| $c_f$ | 0.00243 | 0.00224 | 0.00299 | 0.00219 | 0.00214 | 0.00246 | 0.00263 | 0.00263 | 0.00245 |
| $\Delta c_f$, % | — | −7.8 | 23.0 | −9.9 | −11.9 | 1.2 | 8.2 | 8.2 | 0.8 |
| $c_f Re_\theta^{1/6}$ | 0.012 | 0.011 | 0.015 | 0.011 | 0.010 | 0.012 | 0.013 | 0.013 | 0.012 |

are present, should show acceptable agreement with the available experimental evidence. While we shall elaborate upon these criteria later on, they raise the second question, namely that of selecting the test cases against which all calculations are to be compared. In the present study, attention is focused upon incompressible two-dimensional boundary layers and calculations have been performed for the following test cases:

1) Flat-plate boundary layer by Wieghardt and Tillmann.[28]

2) Equilibrium adverse pressure gradient boundary layer by Andersen et al.[29]

3) Strong favorable pressure gradient (relaminarizing) boundary layers by Simpson and Wallace,[30] Patel and Head,[31] and Badri Narayanan and Ramjee.[32]

4) Sink flow boundary layers by Jones and Launder.[33]

It should be noted that the data from experiments 1 and 3a were also selected as test cases at the 1980-81 Stanford Conference[34] after careful review for completeness and reliability. The choice of the first two for the present work is guided by the first criterion. The relaminarizing and sink flows have been selected because they are obviously dominated by wall proximity and low Reynolds number effects.

## V. Calculation Procedure

The turbulence model equations listed earlier were solved together with the continuity and momentum equations for two-dimensional boundary layers, namely

$$\frac{\partial U}{\partial x}+\frac{\partial V}{\partial y}=0 \tag{33}$$

$$U\frac{\partial U}{\partial x}+V\frac{\partial U}{\partial y}=-\frac{1}{\rho}\frac{\mathrm{d}P}{\mathrm{d}x}+\frac{\partial}{\partial y}\left(\nu\frac{\partial U}{\partial y}-\overline{uv}\right) \tag{34}$$

The numerical method used in an adapted version of the implicit marching procedure of Spalding.[35] One hundred cross-stream grid nodes were used to obtain grid-independent solutions and, for an accurate representation of the large gradients in the vicinity of the wall, roughly half of these were located within $y^+<50$. The streamwise step size was taken as $0.25\Theta$, where $\Theta$ is the momentum thickness. In order to resolve changes in the viscous sublayer, the maximum step size was additionally restricted to five sublayer thicknesses, i.e., $\Delta x<25\nu/u_\tau$. Initial profiles of the mean velocity were obtained by curve fits to the available data. A representative flat-plate distribution was used for the $k$ profile. The initial profile of $\epsilon$ was generated from a formula given by Hassid and Poreh.[36] Further details of the procedure are given in Rodi and Scheuerer.[37]

The calculations were performed on a Burroughs B7700 computer. Computing times were of the order of 0.15 s/step, with only minor differences between the various models, because all involve about the same number of arithmetic operations as can be seen from the equations. This observation is at variance with the findings of HO and CH, who reported large differences in computing times between their models and that of Jones and Launder.

## VI. Results and Discussion

Table 8 and Figs. 3 and 4 show the results of the calculations for the simplest test case, namely the flat-plate boundary layer. The comparisons are limited to the skin-friction coefficient $c_f$, the velocity profiles in wall coordinates, and the distribution of the turbulent kinetic energy in the near-wall region. The skin-friction data in Table 8 were deduced from the measurements of Wieghardt and Tillmann[28] and comparison is made at $x=4.987$ m, which is about 1700 initial boundary-layer thicknesses downstream of the starting location, so that the results are not affected by the initial conditions. In addition, the quantity $c_f Re_\Theta^{1/6}$, which should be approximately constant and equal to 0.012 in a fully turbulent boundary layer, is listed in Table 8. Figure 3 shows the velocity profiles at three stations ($Re_\Theta=5000$, 10,000, 15,000), while Fig. 4 compares the calculated turbulent kinetic energy profiles with the data discussed in Sec. II. It is obvious that there is considerable diversity among the results of the various models.

Table 8 and Fig. 3 show a strong correlation between the ability of a model to reproduce the standard law of the wall and the corresponding prediction of the wall shear stress. Thus, for example, the overshoot in the law of the wall in DM and, to a lesser extent in LS, results in an underestimation of $c_f$. The models of HP, LB, and LB1 confirm this correlation with results in the opposite direction. The HO model gives a very small logarithmic region and rather peculiar profile shapes in the outer layer, due presumably to the use of the large diffusion constants (see Table 1). The best fit to the law of the wall is achieved by CH and WR whose models also predict $c_f$ quite accurately. This consistency is all the more important in establishing the successful features of the models in view of the fact that $c_f$ has been calculated for each case from the slope of the velocity profile at the wall and not by recourse to the logarithmic region.

Figure 4 shows that the shape of the turbulent kinetic energy is better predicted by those models that yield good agreement with respect to the law of the wall and $c_f$, with the exceptions of WR and LS. The former is not surprising in view of the uncertainty concerning the relationship between $k$ and the "mixing energy" in the WR model. The poorer performance of the LS model may be explained by the term $E$ in the model equation, which is likely to increase the dissipation rate $\epsilon$ and therefore reduce $k$ in the vicinity of the wall. It is also apparent from Fig. 4 that none of the models fits the data well, but the results with LB, LB1, and CH show fair agreement with the location and magnitude of the energy maximum. Finally, the results of LB and LB1, obtained with the different $\epsilon$ boundary conditions at the wall discussed earlier, are almost identical. Since the zero-gradient condition at the wall (LB1) is easier to apply in numerical calculations and was found to yield $\epsilon^+$ at the wall in good agreement with the experimental value, this boundary condition has been used in all subsequent calculations with the LB model.

The foregoing results indicate that not all of the available low Reynolds number models reproduce the most basic features of a flat-plate boundary layer. Only the more promising versions of LS, CH, LB1, and WR will therefore be discussed in the context of the remaining test cases.

The results for the equilibrium adverse pressure gradient boundary layer are shown in Fig. 5. The freestream velocity in this experiment was varied according to $U_e \propto x^{-0.15}$, so that only a moderate deceleration occurred. The models by CH and LB overestimate $c_f$, whereas LS and WR yield satisfactory results. It should be noted that slight irregularities existed in the freestream in the experiments of Andersen et al.[29] around $x=0.4$ m. These manifest themselves most strongly in the calculations with the CH model, because there the low Reynolds number functions are linked directly to the mean velocity distribution via the friction velocity. The other models exhibit a more sluggish response to these disturbances, in agreement with the experimental evidence. The equilibrium shape parameter

$$G=\frac{u_\tau}{\delta_l U_e}\int_0^\infty \left(\frac{U_e-U}{u_\tau}\right)^2 \mathrm{d}y \tag{35}$$

where $\delta_l$ is the displacement thickness, is also shown in Fig. 5. All predictions are lower than the experimental values, with the WR model showing the best results. It is interesting to note that all models predict nearly constant values beyond $x=0.6$ m, but a different equilibrium flow is predicted in each case.

The results of the calculations for the three favorable pressure gradient boundary layers are shown in Figs. 6-9. Recall that the low Reynolds number models were constructed primarily to describe such flows, since the accelerations lead to a reduction in the Reynolds number, thickening of the sublayer, and eventual relaminarization. Simpson and Wallace[30] investigated a boundary layer in which the acceleration parameter $K=(\nu/U_e^2)\mathrm{d}U_e/\mathrm{d}x$ was nearly constant and equal to $2.0\times10^{-6}$. This acceleration is not particularly strong and complete relaminarization does not occur. Figure 6 shows the distribution of the skin-friction coefficient and the shape factor. The calculated results are somewhat above the data, the best agreement being achieved by the LS model. For this case the WR model gives the highest skin-friction coefficients. The shape factor exhibits an interesting behavior. The data show an initial decrease as a result of the acceleration up to $x=3$ m and then an increase due to relaminarization. All of the models reproduce this behavior in reasonable agreement with the data. The calculated velocity profiles (Fig. 7) show a departure from the usual law of the wall as indicated by the experiments, but the predicted thickening of the sublayer is not as rapid as that observed in the experiments.

In the case of Patel and Head,[31] the acceleration is more severe. Figure 8 shows that the models reproduce the initial increase in $c_f$ and the subsequent decrease, associated with relaminarization, quite well. Only the model of LS gives slightly lower skin-friction coefficients. The accompanying decrease and increase in the shape parameter, not shown here, is also predicted with satisfactory accuracy.

The reversion to a quasilaminar state has been investigated in the experiments of Badri Narayanan and Ramjee,[32] where values of the acceleration parameter $K$ of up to $7\times10^{-6}$ were attained. Figure 9 compares the calculated and measured skin-friction coefficients, which display a drastic decrease due to the strong acceleration. The LS model predicts this variation satisfactorily, while the others reproduce only the qualitative features.

The final comparison was made with the sink flow data of Jones and Launder,[33] which correspond to a constant value of the acceleration parameter $K=1.5\times10^{-6}$. Under these conditions, the boundary layer shows similarity behavior with a constant skin-friction coefficient, shape parameter, and momentum thickness Reynolds number. The measured values of these quantities are compared with the calculations

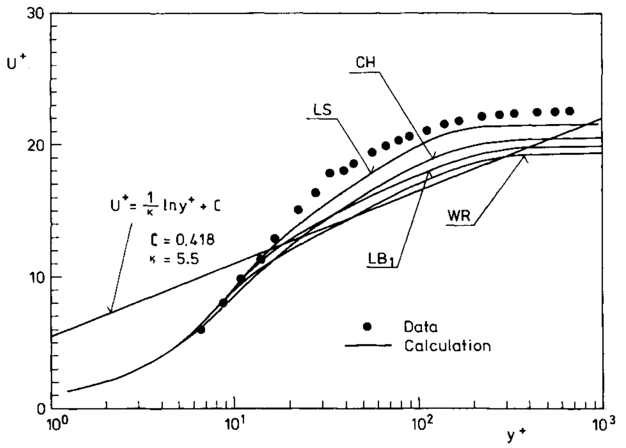


**Fig. 7 Velocity profile at $x=4.604$ m for the experiment of Simpson and Wallace.[30]**

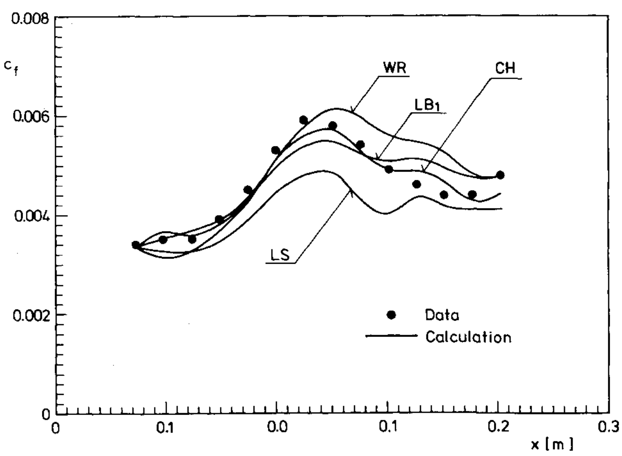


**Fig. 8 Comparison of model results with the data of Patel and Head.[31]**

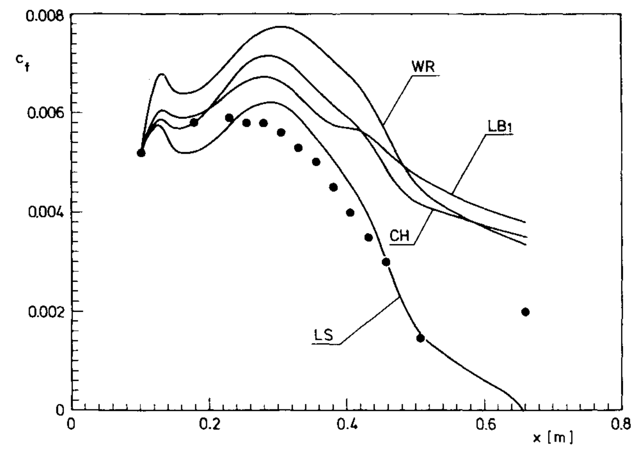


**Fig. 9 Comparison of model results with the data of Badri Narayanan and Ramjee.[32]**

**Table 9 Skin-friction coefficients, Reynolds numbers, and shape factors for the sink flow experiments of Jones and Launder[33]**

| Quantity | Experiment | LS | CH | LB1 | WR |
|---|---|---|---|---|---|
| $c_f$ | 0.0046-0.0056 | 0.00424 | 0.00478 | 0.0050 | 0.00525 |
| $Re_\theta$ | 640 | 578 | 656 | 699 | 731 |
| $H$ | 1.470 | 1.482 | 1.440 | 1.380 | 1.389 |

in Table 9. The models of LB and WR give fairly high $c_f$ values and accordingly low shape factors. The opposite is true for the LS model. The best representation of the data is achieved by the CH model for this case.

## VII. Conclusions

The results presented here are somewhat limited with respect to details such as velocity profile shapes and turbulence parameters. Nevertheless, they are sufficient to indicate clearly the relative performance of the various models proposed to describe near-wall flows. It is apparent that not all of the models considered here yield satisfactory results. The proposals of HP, HO, DM (and RE) fail to reproduce even the simplest test case, namely the flat-plate boundary layer. It is interesting to note that already in Sec. III these models were considered unsatisfactory on physical grounds. From an overall examination of the results for all the test cases, it appears that the models of Launder and Sharma[17] and, to some extent, Chien[12] and Lam and Bremhorst,[16] which are based on the $k$-$\epsilon$ model, and that of Wilcox and Rubesin[19] yield comparable results and perform considerably better than the others. However, even these need further refinement if they are to be used with confidence to calculate near-wall and low Reynolds number flows. The calculations and the theoretical considerations in Sec. III suggest that the performance of these models can be improved by 1) selecting a damping function $f_\mu$ for the shear stress that is in agreement with experimental evidence and whose influence is restricted to the sublayer and buffer zone; 2) choosing the low Reynolds number functions $f_1$ and $f_2$ in the dissipation rate equation with a mathematically consistent near-wall behavior and, if possible, in accordance with empirical information; and 3) fine tuning the functions to ensure the reproduction of the well-known basic features of wall-bounded shear flows over a range of pressure gradients. A distinct improvement of the predictions for adverse pressure gradient flows will require additional modifications of the high Reynolds number models.

## Acknowledgments

Part of this research was performed while the first author was on a Faculty Development Leave from The University of Iowa at the Institut für Hydromechanik of the University of Karlsruhe as a recipient of the Senior U.S. Scientist Award of the Alexander von Humboldt Foundation. The support of all three institutions is gratefully acknowledged. The authors are also grateful to Ms. Michaela Laternik for typing the manuscript so efficiently.

## References

[1]van Driest, E. R., "On Turbulent Flow Near a Wall," *Journal of the Aeronautical Sciences*, Vol. 23, 1956, pp. 1007-1011.

[2]Coles, D., "A Model for Flow in the Viscous Sublayer," *Proceedings of the Workshop on Coherent Structure of Turbulent Boundary Layers*, Lehigh University, Bethlehem, Pa., 1978.

[3]El Telbany, M. M. M. and Reynolds, A. J., "Turbulence in Plane Channel Flows," *Journal of Fluid Mechanics*, Vol. 111, 1981, pp. 283-318.

[4]Hinze, J. O., *Turbulence*, 2nd ed., McGraw Hill Book Co., New York, 1975.

[5]Launder, B. E., "Second Moment Closure: Methodology and Practice," *Proceedings of the Ecole d' Eté d' Analyse Numerique-Modelisation Numerique de la Turbulence*, Clamart, France, 1982.

[6]Kreplin, H.-P. and Eckelmann, H., "Behaviour of the Three Fluctuating Velocity Components in the Wall Region of a Turbulent Channel Flow," *Physics of Fluids*, Vol. 22, 1979, pp. 1233-1239.

[7]Sirkar, K. K. and Hanratty, T. J., "The Limiting Behaviour of the Turbulent Transverse Velocity Component Close to a Wall," *Journal of Fluid Mechanics*, Vol. 44, 1970, pp. 605-614.

[8]Derksen, R. W. and Azad, R. S., "Behaviour of the Turbulent Energy Equation at a Fixed Boundary," *AIAA Journal*, Vol. 19, 1981, pp. 238-239.

[9]Rotta, J. C., "Turbulent Boundary Layers in Incompressible Flow," *Progress in the Aeronautical Sciences*, Vol. 2, 1962, pp. 1-219.

[10]Schubauer, G. B., "Turbulent Processes as Observed in Boundary Layer and Pipe," *Journal of Applied Physics*, Vol. 25, 1954, pp. 188-196.

[11]Laufer, J., "The Structure of Turbulence in Fully Developed Pipe Flow," NACA Rept. 1174, 1954.

[12]Chien, K.-Y., "Predictions of Channel and Boundary-Layer Flows with a Low-Reynolds-Number Turbulence Model," *AIAA Journal*, Vol. 20, Jan. 1982, pp. 33-38.

[13]Dutoya, D. and Michard, P., "A Program for Calculating Boundary Layers along Compressor and Turbine Blades," *Numerical Methods in Heat Transfer*, edited by R. W. Lewis, K. Morgan, and O. C. Zienkiewicz, John Wiley & Sons, New York, 1981.

[14]Hassid, S. and Poreh, M., "A Turbulent Energy Dissipation Model for Flows with Drag Reduction," *Journal of Fluids Engineering*, Vol. 100, 1978, pp. 107-112.

[15]Hoffmann, G. H., "Improved Form of the Low-Reynolds Number $k$-$\epsilon$-Turbulence Model," *Physics of Fluids*, Vol. 18, 1975, pp. 309-312.

[16]Lam, C. K. G. and Bremhorst, K. A., "Modified Form of the $k$-$\epsilon$-Model for Predicting Wall Turbulence," *Journal of Fluids Engineering*, Vol. 103, 1981, pp. 456-460.

[17]Launder, B. E. and Sharma, B. I., "Application of the Energy-Dissipation Model of Turbulence to the Calculation of Flow Near a Spinning Disc," *Letters in Heat and Mass Transfer*, Vol. 1, 1974, pp. 131-138.

[18]Reynolds, W. C., "Computation of Turbulent Flows," *Annual Review of Fluid Mechanics*, Vol. 8, 1976, pp. 183-208.

[19]Wilcox, D. C. and Rubesin, W. M., "Progress in Turbulence Modeling for Complex Flow Fields Including Effects of Compressibility," NASA Tech. Paper 1517, 1980.

[20]Jones, W. P. and Launder, B. E., "The Prediction of Laminarization with a Two-Equation Model of Turbulence," *International Journal of Heat and Mass Transfer*, Vol. 15, 1972, pp. 301-314.

[21]Hanjalic, K. and Launder, B. E., "Contribution Towards a Reynolds-Stress Closure for Low-Reynolds-Number Turbulence," *Journal of Fluid Mechanics*, Vol. 74, 1976, pp. 593-610.

[22]Rodi, W., "Turbulence Models and their Application in Hydraulics," International Association of Hydraulic Research, Monograph, Delft, the Netherlands, 1980.

[23]Launder, B. E., Morse, A., Rodi, W., and Spalding, D. B., "A Comparison of the Performance of Six Turbulence Models," NASA SP-321, 1972.

[24]Rodi, W., "A Review of Experimental Data of Uniform Density Free Turbulent Boundary Layers," *Studies in Convection*, edited by B. E. Launder, Academic Press, London, 1975, pp. 79-165.

[25]Launder, B. E., "Progress in the Modeling of Turbulent Transport," von Kármán Institute, Rhode-Saint Genese, France, Lecture Series 76, 1975.

[26]Batchelor, C. K. and Townsend, A. A., "Decay of Isotropic Turbulence in the Final Period," *Proceedings of the Royal Society of London*, Ser. A, Vol. 194, 1948, p. 538.

[27]Chambers, T. L. and Wilcox, D. C., "Critical Examination of Two-Equation Turbulence Closure Models for Boundary Layers," *AIAA Journal*, Vol. 15, 1977, pp. 821-828.

[28]Wieghardt, K. and Tillmann, W., "On the Turbulent Friction Layer for Rising Pressure," NACA TM 1314, 1951.

[29]Andersen, P. S., Kays, W. M., and Moffat, R. J., "The Turbulent Boundary Layer on a Porous Plate: An Experimental Study of the Fluid Mechanics for Adverse Free-Stream Pressure Gradients," Dept. of Mechanical Engineering, Thermosciences Div., Stanford University, Stanford, Calif., Rept. HMT-15, 1972.

[30]Simpson, R. L. and Wallace, D. B., "Laminarescent Turbulent Boundary Layers: Experiments on Sink Flows," Project SQUID, Tech. Rept. SMU-1-PU, 1975.

[31]Patel, V. C. and Head, M. R., "Reversion of Turbulent to Laminar Flow," *Journal of Fluid Mechanics*, Vol. 34, 1968, p. 371.

[32]Badri Narayanan, M. A. and Ramjee, V., "On the Criteria for Reverse Transition in a Two-Dimensional Boundary Layer Flow," *Journal of Fluid Mechanics*, Vol. 35, 1969, p. 225.

[33]Jones, W. P. and Launder, B. E., "Some Properties of Sink-Flow Turbulent Boundary Layers," *Journal of Fluid Mechanics*, Vol. 56, 1972, pp. 337-351.

[34]Kline, S. J., Cantwell, B. J., and Lilley, G. M., "Comparison of Computation and Experiment," *The 1980-81 AFOSR-HTTM-Stanford Conference on Complex Turbulent Flows*, Vol. I, Mechanical Engineering Dept., Thermosciences Div., Stanford University, Stanford, Calif., 1981.

[35]Spalding, D. B., *GENMIX—A General Computer Program for Two-Dimensional Parabolic Phenomena*, Pergamon Press, Oxford, England, 1977.

[36]Hassid, S. and Poreh, M., "A Turbulent Energy Model for Flows with Drag Reduction," *Journal of Fluids Engineering*, Vol. 97, 1975, pp. 234-241.

[37]Rodi, W. and Scheuerer, G., "ALFA—Ein Programm zur Berechnung der Wärmeübergangszahlen an Gasturbinenschaufeln," *Forschungsvereinigung Verbrennungskraftmaschinen*, Heft 326-1, 1983.